WELDING PROCESS SIMULATION WITH SIMULTANEOUS COMPUTATION OF MATERIAL PROPERTIES

A. Anca, A. Cardona and J.M. Risso

Centro Internacional de Métodos Computacionales en Ingeniería (CIMEC)
INTEC - UNL - CONICET
Parque Tecnológico del Litoral Centro
(3000) Santa Fe, Argentina
e-mail: aanca@intec.unl.edu.ar

Key Words: Welding Simulation, Thermal Stresses, Metallurgical Transformations.

Abstract. *Residual stresses and plastic strains are produced by localized heating and cooling during welding. These stresses can lead to distortion and under certain circumstances even the premature failure of welded parts. Thus, residual stresses play an important role as far as the quality and reliability of a welded construction are concerned.*

Formation of distortions and residual stresses in weldments depend on many interrelated factors such as thermal and mechanical fields, phase transformations, material properties, structural boundary conditions, types of welding operation and welding conditions[1,2]

In the present work, the previous finite element model developed by the authors[3] to study the thermomechanical behavior of the solidifying metal in welding processes is validated using the analytical solution of Weiner and Boley.[4]

Also a kinetics based model was integrated into the same multiphysics finite element program to provide the time evolution of the microstructure.[5] The material properties required for the non-linear thermomechanical analysis are temperature and phase dependent, and this dependency is accounted for by computing the microstructure evolution and using this information to estimate the material properties. This is done by assigning temperature dependent material properties to each phase and applying mixture rules to predict macro material properties.

Finally numerical results are presented to illustrate the evolution of the stress field in a buttwelded joint.

1   INTRODUCTION

Various interacting factors, including thermal, mechanical and metallurgical ones, are recognized to be the cause of welding problems. In order to predict distortions, residual stresses and mechanical properties of the welded joint, a coupled thermal-metallurgical-mechanical analysis must be done. In a previous work[3] we focused on the development of a reliable thermal model with ability to track the evolution of the phase-change problem, validating it against analytic formulations.[6] In this paper we analyze the evolution of the material microstructure, the strain field and the stress field during steel welding processes. A description of the metallurgical model used to compute thermophysical properties is detailed in section 2. In section 3 we develop an improved 3D formulation to solve the thermal-mechanical problem. In section 4 we compare the results obtained using this model with the semi-analytical solution of Weiner and Boley,[4] a validation benchmark widely used to test formulations for continuous casting simulation.[7,8] Finally, in section 6 we present numerical results of simulation of a butt weld, obtained by using the proposed coupled thermo-metallurgical-mechanical model.

2   METALLURGICAL MATERIAL MODEL

Welding operations in steel involve solid state structural transformations. Austenite will form during heating if the temperature becomes higher enough than Ac3 and it will decompose during cooling below Ar3. Depending on cooling rate ferrite, pearlite, bainite and/or martensite will be formed. These transformations generate thermal, metallurgical and mechanical phenomena in the material, some of which are:

- changes in thermal properties of the material

- changes in mechanical properties of the material

- changes in isotropic specific volume between parent and product phases.

This makes the material properties dependent on temperature and temperature history.

The method we used in this work to account for the temperature dependency of the material properties is to calculate microstructure evolution and assign temperature dependent material properties to each phase. The phase properties are combined using a linear mixture rule to obtain macro material properties.

2.1   Modelling Solid-State phase transformations in metals

In the present work only solid state transformations that occur during the cooling stage of welding processes are accounted for. We use data obtained from isothermal Temperature-Time-Transformation (IT) curves to predict the evolution of transformations during continuous cooling.

Austenite decomposition into ferrite, pearlite or bainite is driven mainly by diffusion of carbon atoms, and is therefore said to be a diffusive transformation. This case is described by an isothermal Avrami-type[9,10] evolution law (also known as Johnson-Mehl-Avrami-Kolmogorov

or JMAK law). The use of this equation to calculate the fraction transformed during cooling is related with the Scheil's additivity rule,[11] which states that the fraction which transforms at any given temperature is a function only of the proportion of the metal already transformed and the temperature T.

The diffusionless transformation from austenite to martensite takes place at the highest cooling rates and it is described by the Koistinen-Marburger formulae.

2.1.1 Diffusive kinetics

The kinetics of diffusion-controlled transformations was extended by Jones and Bhadeshia[12] and followed by other authors (e.g. Reti et. al.[13]) to model austenite multi-phase decomposition.

For an isothermal transformation at temperature T the volume fraction y_i of the product constituent k at time t is:

$$y_k(t) = Y_k(t) \left[1 - \exp\left(-B_k t^{m_k}\right) \right], \tag{1}$$

$$\tag{2}$$

where B_k, m_k and Y_k are parameters that depend on the temperature T; and k (ferrite, pearlite, bainite) are phase products involved in the reaction.

The coefficients $B_i = B_i(T)$ and $m_i = m_i(T)$ can be determined from isothermal transformation diagrams (IT-diagrams) providing the start and final transformation times for a giving temperature. The parameter $Y_i = Y_i(T)$ is the maximum volume fraction of the precipitating phase i that follows an isothermal transformation at temperature T and has to be determined experimentally.

2.1.2 Martensite kinetics

During cooling, when the temperature reaches the M_s temperature, austenite starts to transform into martensite.

The martensitic volume fraction is usually described by the Koistinen-Marburger law:

$$y_m = Y_m \left(1 - \exp\left(-\widetilde{k}(M_s - T)\right) \right), \qquad T < M_s, \tag{3}$$

where Y_m is the residual volume fraction of austenite at M_s, and $\widetilde{k}$ describes the martensitic development as function of temperature ($\widetilde{k} = 0.011$ for steels).

2.1.3 The additivity-rule

We based our approach on the additivity rule, where cooling curve is divided into successive isothermal steps.

From the fraction y_k^i transformed at the end of the time step t^i, the new transformed fraction at the end of this step ($t^{i+1} = t^i + \Delta t^{i+1}$) is determined by

$$y_k^{i+1} = Y_k^{i+1} \left(1 - \exp\left(-B_k^{i+1}(\hat{t}^i + \Delta t^{i+1})^{m_k^{i+1}} \right) \right),$$ (4)

where parameters are evaluated at T^{i+1} and in which $\hat{t}^i$ is a fictitious time defined as:

$$\hat{t}^i = \left(-\frac{\ln\left(1 - \frac{y_k^i}{Y_k^{i+1}} \right)}{B_k^{i+1}} \right)^{1/m_k^{i+1}}$$ (5)

2.1.4 CCT-diagrams

As an example of the implemented formulation, we present here the calculation of a CCT diagram. Taking as input an isothermal transformation diagram (figure 1) that describes ferritic and pearlitic transformations, and applying the multi-phase transformation model for different constant cooling rates ($\dot{T} = constant$) we obtain a continuous cooling transformation diagram shown in figure 2. The same data is used later in the welding numerical example.
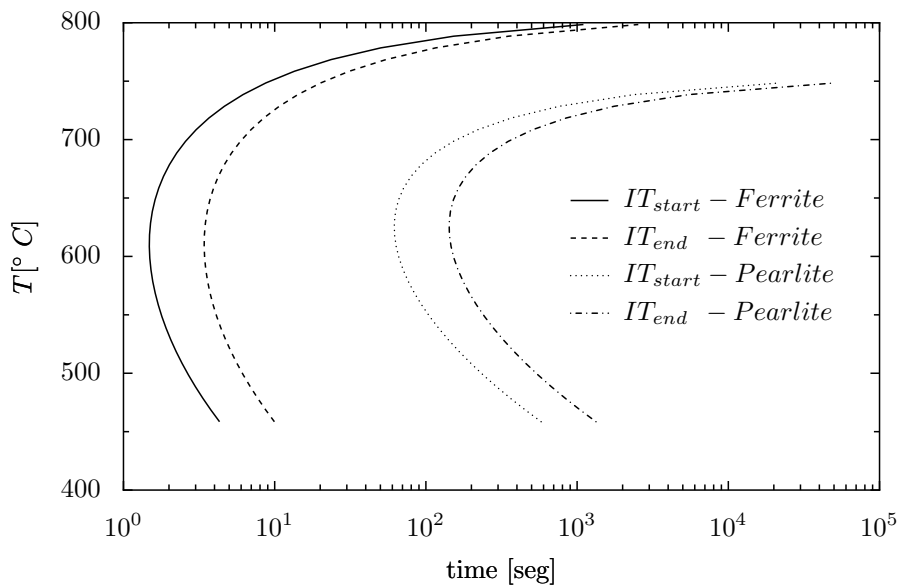

Figure 1: IT-diagram

The computed phase fractions vs. time for multi-phase isothermal transformations are also plotted on figure 3.
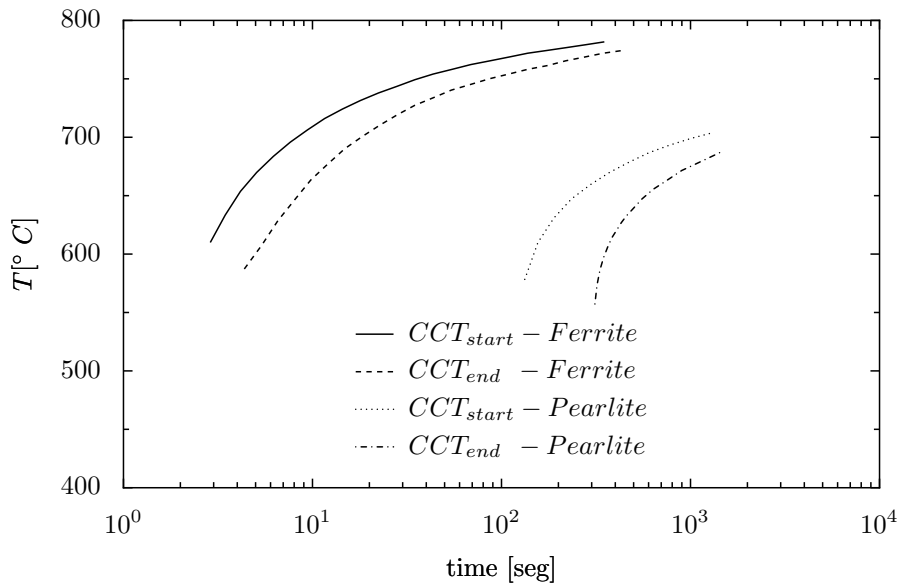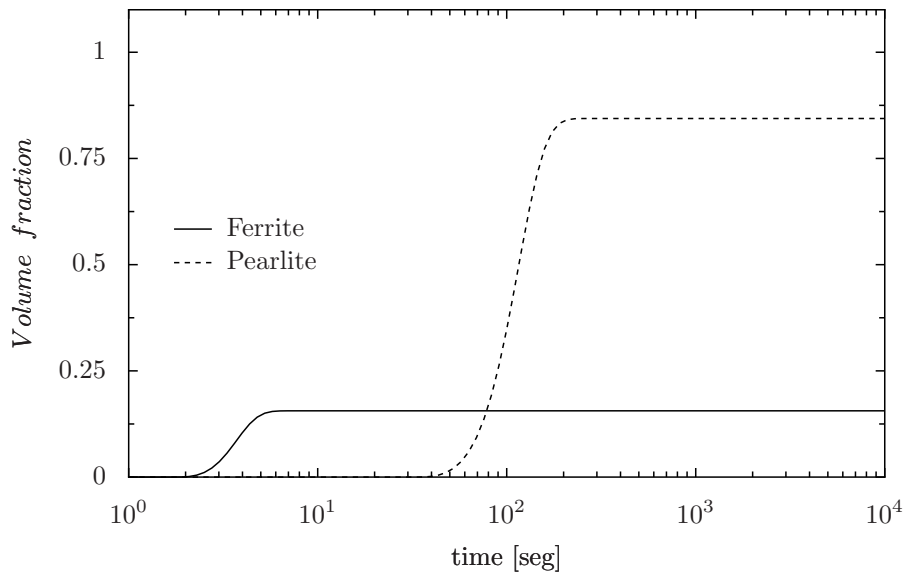
Figure 2: CCT-diagram

Figure 3: Isothermal evolution of phase fractions of ferrite and pearlite at $650°C$

2.2   Mixture Rules and Material Properties

The material properties are computed by assigning temperature dependent properties to each phase. They are combined by using linear mixture rules to obtain macro materials properties. The general formula for overall macro properties based on the properties for the different k phases is

$$\hat{P}(T,t) = \sum_k y_k(T,t)\hat{p}_k(T) \tag{6}$$

where y_k = volume fraction of phase k; $\hat{p}_k$ = material property for phase k; $\hat{P}$ = macro property.

The material properties computed by the mixture rule are heat capacity, heat conductivity, Young modulus, yield limit, hardening modulus, thermal expansion coefficient and Poisson ratio.

An instantaneous austenization model was assumed. Therefore no other solid-state phase than austenite will exist above Ac3 temperature.

2.3 Algorithmic implementation

The present metallurgical model was coded in OOFELIE *Object Oriented Finite Elements Led by an Interactive Executor*.[14, 15]

Each *Element* class in OOFELIE toolkit includes an instance of the *State* class, where state variables are stored (e.g. temperatures, phase fractions, time, equivalent plastic strain, and in general any historical value), and then passed as arguments to the *Material* class methods.

Following the Object Oriented Programming (OOP) philosophy, a new *MetallurgicalMaterial* class was derived from the base *Material* class (see figure 4). An instance of this class contains all the information related to IT diagrams (*TTT_Diagram* class) and provides methods to do phase fractions computations (*getPhaseFractions(state)*). In turn, this *MetallurgicalMaterial* class has pointers to an already instantiated *SingleMetallurgicalMaterial* object, which contains material data corresponding to parent and product phases. In this way, using polimorphism and overloading the model can be used either with thermal or mechanical elements. Because the information is fully encapsulated an Element can call safely the member function *get(state)* knowing that a suitable technique will be automatically used to calculate the desired property using equation (6).

3 DESCRIPTION OF THE MECHANICAL PROBLEM

Due to the localized nature of the heat application during a thermal welding process, the area surrounding the seam (usually known as heat affected zone, HAZ) is subjected to expansion/contraction, microstructural transformations and melting/solidifying processes that lead to plastic strains, which results in undesired residual stresses and permanent deformations.

Thermal strains and stresses in the solid phase will be treated in this section assuming a transient condition for the thermal problem uncoupled from the mechanical variables. Inertial effects are ignored in momentum balance equations, according to the assumption of null velocity field within the solid.

After determining the temperature field and microstructural evolution, we make a stress analysis considering a nonlinear material behavior with parameters strongly dependent on temperature and microstructure.
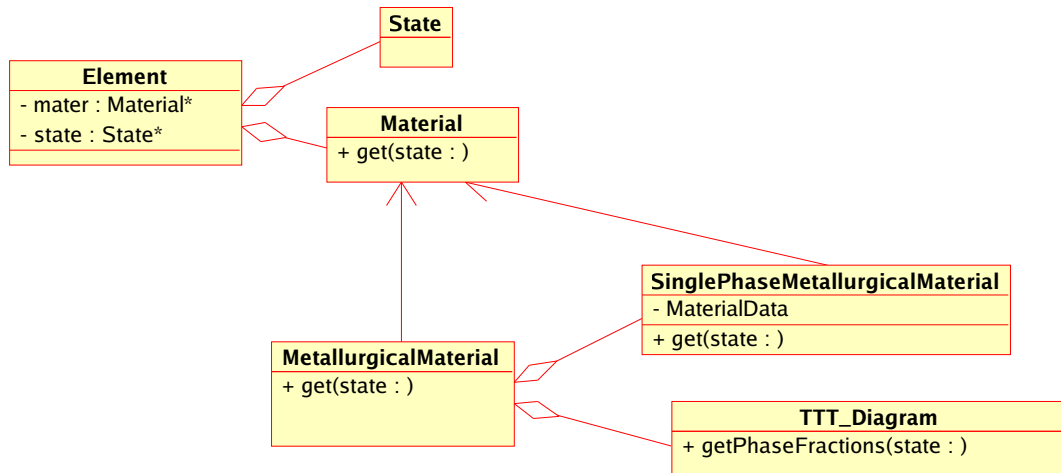
Figure 4: Class diagram

It is recognized that finite element techniques with standard constitutive material modelling yield good solutions in thermal stress analysis even when the solid is subjected to temperatures near the solidification ones. However, there are particular aspects in the formulation for melting/solidifying problems that need to be carefully considered.

For the mechanical simulation of this process we consider three different configurations for every material point and its neighborhood (figure 5):

i) the reference configuration (B), in which the particle label is assigned;

ii) the (intermediate) natural configuration (B^0) which corresponds to that state where the material point solidified just below the zero strength temperature (ZST), and started to develop mechanical strength;

iii) the current configuration (B^t).

Note that, since the solidification time instant is not the same one for all points in the domain of analysis, each material point has its own (intermediate) natural configuration.

Defining $\mathbf{u}^o$ as the displacement from the reference to the natural configuration, $\mathbf{u}^t$ the displacement from the reference to the current configuration and $\mathbf{u}$ the displacement from the natural to the current configuration, we can write:

$$\mathbf{u}^t = \mathbf{u} + \mathbf{u}^o \tag{7}$$

Usually, when a finite element procedure is used, the mesh is defined in the reference configuration (the set of points at time $t = 0$) as depicted schematically in figure 5-b.

Let us consider that $\mathbf{X}$ and $\mathbf{x}^o$ are coordinate systems in the reference and natural configurations, respectively. As a consequence of the assumption of small deformations we introduced to describe motion, and by assuming the existence of the intermediate deformation gradient in the
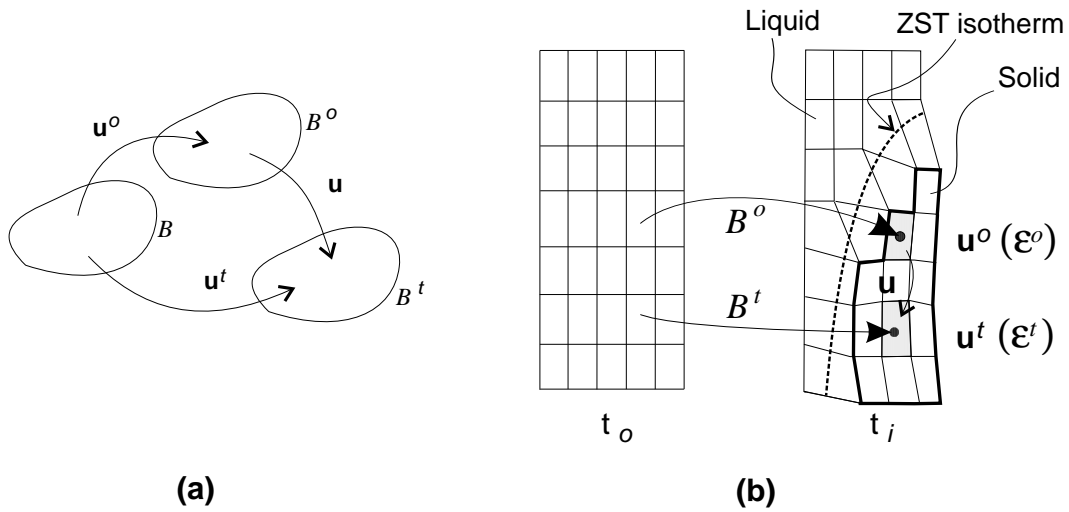
Figure 5: Reference (B), natural (B^0) and current (B^t) body configurations in the solidification problem

neighborhood of every point, we have: $\nabla_{\mathbf{X}}\mathbf{x}^o \approx \mathbf{1}$ The same assumption allows us to evaluate the strain $\boldsymbol{\varepsilon} = \nabla_{\mathbf{x}^o}^{sym}\mathbf{u}$, related to the motion from the natural to the final configurations, by the following approximation:

$$\boldsymbol{\varepsilon} = \nabla_{\mathbf{x}^o}^{sym}\mathbf{u} \approx \nabla_{\mathbf{X}}^{sym}\mathbf{u} \tag{8}$$

By taking gradients in equation (7) and using the assumptions stated above, we can verify the validity of the additive decomposition of strains:

$$\boldsymbol{\varepsilon}^t = \boldsymbol{\varepsilon} + \boldsymbol{\varepsilon}^o \tag{9}$$

where $\boldsymbol{\varepsilon}^t = \nabla_{\mathbf{X}}^{sym}\mathbf{u}^t$ is the strain tensor at the actual configuration (time t) with respect to the reference configuration, and $\boldsymbol{\varepsilon}^o = \nabla_{\mathbf{X}}^{sym}\mathbf{u}^o$ is the strain at the natural configuration with respect to the reference one.

The mechanical strain $\boldsymbol{\varepsilon}_M$ is computed subtracting the thermal strain $\boldsymbol{\varepsilon}_T$ from the actual strain $\boldsymbol{\varepsilon}$:

$$\boldsymbol{\varepsilon}_M = \boldsymbol{\varepsilon} - \boldsymbol{\varepsilon}_T \qquad ; \qquad \boldsymbol{\varepsilon}_T = \beta(T)\mathbf{1} \tag{10}$$

with $\beta(T)$ being the thermal expansion function.

Stresses in the solid shell are directly related to the mechanical strains through the constitutive material law.

To test the formulation we selected a standard elastoplastic model, based in the classical J_2 theory with isotropic hardening[16] and the von Mises yield criteria.

We remark that for a correct representation of the steel constitutive behavior in the zone of interest, it is mandatory to account for the strong dependence of the material parameters on temperature.
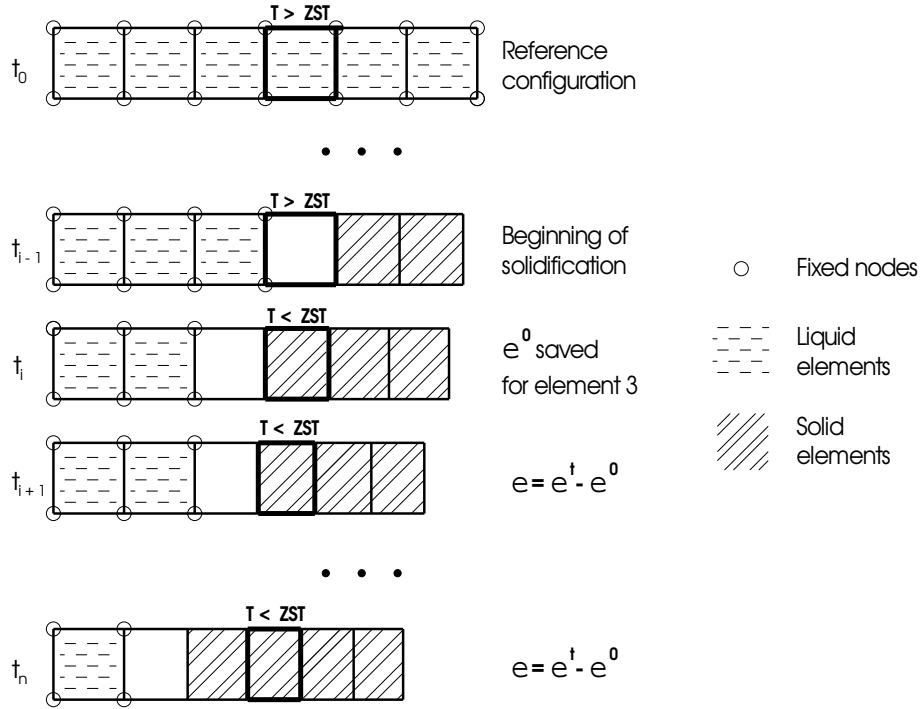
Figure 6: Evolution of d.o.f.s and strains in solidification problems

3.1 Finite element implementation

The standard quasi-static boundary value problem in solid mechanics, stated in mixed $\boldsymbol{u}$-p form,[17] consists in finding the displacement field $\boldsymbol{u}$ and the mean-stress field p that satisfy the integral equations

$$\int_\Omega \operatorname{tr}\left(\boldsymbol{\sigma}_{dev}\operatorname{grad}\boldsymbol{w}\right)\mathrm{d}V + \int_\Omega p\operatorname{div}\boldsymbol{w}\,\mathrm{d}V = \int_\Omega \rho\boldsymbol{b}\cdot\boldsymbol{w}\,\mathrm{d}V + \int_{\partial\Omega_\sigma}\bar{\boldsymbol{t}}\cdot\boldsymbol{w}\,\mathrm{d}S, \qquad (11)$$

$$\int_\Omega \left[\operatorname{tr}\left(\boldsymbol{\varepsilon}_M\right) - \frac{p}{\kappa}\right]q\,\mathrm{d}V = 0, \qquad (12)$$

throughout the domain Ω, for all the admissible displacement and mean-stress weighting functions $\boldsymbol{w}$ and q, respectively.

Equation (11) is the weak form of the momentum balance equations, where $\rho\boldsymbol{b}$ is the body-force (per unit volume) and $\bar{\boldsymbol{t}}$ is the traction prescribed over the portion $\partial\Omega_\sigma$ of the boundary (displacement boundary conditions over the complementary portion $\partial\Omega_u$ are assumed to hold a priori).

Appropriate mixed finite elements should be employed in order to deal with the numerical difficulties eventually caused by the inelastically-incompressible behavior of metals. We refer to the classical finite element literature[17,18] for a detailed discussion of admissible $\boldsymbol{u}$- and p-shape functions that guarantee the fulfillment of the Babuška-Brezzi stability conditions.

The displacement and mean-stress trial functions are defined as follows:

$$\boldsymbol{u} = \sum_{i=1}^{n_u} N_i \boldsymbol{U}_i = \boldsymbol{N}\boldsymbol{U}, \tag{13}$$

$$p = \sum_{j=1}^{n_p} N_{p\,j} P_j = \boldsymbol{N}_p \boldsymbol{P}, \tag{14}$$

N_i being the displacement shape function associated to the displacement node $i = 1, 2, \ldots, n_u$, $\boldsymbol{U}_i$ the nodal displacement, $N_{p\,j}$ the mean-stress shape function associated to the mean-stress node $j = 1, 2, \ldots, n_p$, and P_j the nodal mean stress.

After replacing $\boldsymbol{u}$ and p by their respective finite element approximations, and by adopting the corresponding shape functions as weight functions (Galerkin formulation), it yields

$$\boldsymbol{R}_1 = \boldsymbol{F}_{int} - \boldsymbol{F}_{ext} = \boldsymbol{0}, \tag{15}$$

$$\boldsymbol{R}_2 = \boldsymbol{K}_p^T \boldsymbol{U} - \boldsymbol{M}_p \boldsymbol{P} = \boldsymbol{0}, \tag{16}$$

where

$$\boldsymbol{F}_{int} = \int_\Omega \boldsymbol{B}^T \boldsymbol{\sigma}_{dev} \, \mathrm{d}V + \boldsymbol{K}_p \boldsymbol{P}, \tag{17}$$

$$\boldsymbol{F}_{ext} = \int_\Omega \boldsymbol{N}^T \rho \boldsymbol{b} \, \mathrm{d}V + \int_{\partial\Omega_\sigma} \boldsymbol{N}^T \bar{\boldsymbol{t}} \, \mathrm{d}S, \tag{18}$$

$$\boldsymbol{K}_p = \int_\Omega \boldsymbol{B}^T \boldsymbol{1} \boldsymbol{N}_p \, \mathrm{d}V, \tag{19}$$

$$\boldsymbol{M}_p = \int_\Omega \frac{1}{\kappa} \boldsymbol{N}_p^T \boldsymbol{N}_p \, \mathrm{d}V, \tag{20}$$

$$\tag{21}$$

In the above equations, symmetric second order tensors like the stress deviator $\boldsymbol{\sigma}_{dev}$ and the unit tensor $\boldsymbol{1}$ are mapped into vectors as usually done in the finite element practice, and $\boldsymbol{B}$ is the typical finite element matrix defining the the shape functions derivative.

We implemented this formulation using the C++ templates technique. Only one code was written for all topologies, including linear and quadratic tetrahedron and hexahedron elements. As pointed out by Lindgren,[19,20] hexahedral elements are superior to linear tetrahedral elements, and also better than quadratic tetrahedron elements when plastic deformation occurs, and therefore we used hexahedral elements to do the tests.

The discrete equilibrium equations are solved by using a standard Newton-Raphson method. The Jacobian matrix corresponds to that obtained from an equivalent purely Lagrangian elastoplastic quasi-static incremental problem (see for instance Simo et al.[16]).

Remarks:

- The strain ε^o is computed the first time that all nodal temperatures of the considered element fall below the zero strength temperature (ZST), and is stored at the finite element Gauss point as an additional tensorial internal variable. The *Zero Strength Temperature* is defined as the minimum temperature amongst those at which strength is zero.[21] Temperatures corresponding to solid fraction values ranging from 0.65 to 0.80 are commonly used for this parameter in the literature.[22–24]

- In this model, the solid phase domain changes with time. This fact introduces some difficulties concerning the mesh definition for the FE analysis. The procedure we have implemented consists in defining a mesh that describes the complete domain, including the liquid and mushy zones. Nodes in the liquid and mushy zones are initially fixed. In subsequent time steps, when the nodal temperatures fall below the ZST, nodal d.o.f.'s are freed and the stiffness contribution of the solidified zone is taken into consideration (see figure 6).

- The described numerical model does not predict the real displacement field inside the solid phase, because the displacement field of the natural configuration is not recorded. However, displacements in the natural configuration of the elements located on the solid surface are known and equal to zero, so the real displacements of the solid surface are correctly approximated.

- The technique of subtraction of the strain term ε^o from the total strain ε^t must be emphasized for its simplicity and accuracy. Stress computations based on total strain, without subtraction of the initial strain ε^o, give completely unrealistic results, a fact that may be verified by comparison with results obtained by using the semi-analytical formulation of Weiner et al. We note also that this approach is less expensive than that used by other authors based on recording flow strain for liquid elements.[25]

4   VALIDATION OF THE MECHANICAL MODEL

The thermal stress calculated by the finite element model developed in the present work has been compared with the semi- analytical solution developed by Weiner and Boley[4] for thermal stresses during one-dimensional solidification of a semi-infinite elastic perfectly plastic body after a sudden decrease in surface temperature.

   The thermal problem they solved corresponds to the Neumann's classical one, a phase change 1D problem with uniform initial temperature T_s (solidification temperature) and fixed temperature $T_w < T_s$ on one end, being $T^o = T_s - T_w$ defined as the temperature drop.

   They took an elastic-perfectly plastic material model for the mechanical problem, with a constant Young modulus E and yield stress σ_y varying linearly with temperature:

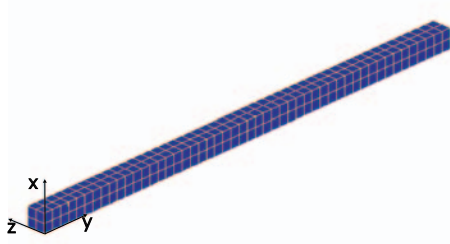$$\sigma_{y(T)} = \sigma_y^o \frac{T_s - T}{T^o} \qquad ; \qquad T \leq T_s \tag{22}$$

Figure 7: Finite element model for the 1-D numerical validation test).

where σ_y^o is the yield stress at temperature T^o.

The Neumann's solution introduces a characteristic length $\bar{y} = p\sqrt{t}$, where t denotes time and the parameter p is given by:

$$p = 2\sqrt{K_s}\gamma \quad ; \quad K_s = \frac{\kappa}{\rho C_p} \quad ; \quad \gamma \approx \sqrt{\frac{T^o C_p}{2L}} \qquad (\gamma^2 \ll 1); \qquad (23)$$

The thermal diffusivity K_s is the ratio of conductivity κ to density ρ and specific heat C_p, while L is the latent heat.

Weiner et al. introduced also the dimensionless quantities:

$$\hat{y} = \frac{y}{\bar{y}} \qquad ; \qquad \hat{T} = \frac{T - T_s}{T^o}$$

$$\hat{\sigma} = \frac{(1-\nu)\sigma}{\alpha E T^o} \quad ; \quad \hat{\sigma}_y = \frac{(1-\nu)\sigma_y}{\alpha E T^o} = -m\hat{T} \quad ; \quad m = \frac{(1-\nu)\sigma_y^o}{\alpha E T^o}$$

where α is the thermal expansion coefficient and ν the Poisson ratio.

We have solved this problem in a prismatic domain using the finite element procedure described in subsection 3, and imposing Extended Plane Strain (EPS) Conditions along transversal directions z and x, to be consistent with the original hypothesis proposed by Weiner et al.

The FE mesh consists in hexahedral elements, as shown in figure 7. The EPS conditions ($\varepsilon_x = $ constant $\varepsilon_z = $ constant) are imposed via Lagrange multipliers, constraining all nodal x- and z-displacements to be identical.

Figure 8 compares the semi-analytical results with the numerical ones. The curves plot the non-dimensional stress component $\hat{\sigma}_{xx}(= \hat{\sigma}_{zz})$ along the non-dimensional $\hat{y}$-line (longitudinal direction) for $m = 0.097$ and $\gamma = 0.465$. The agreement of the numerical FE solution with the semi-analytical one is evident from the figure.

It should be noted that this semi-analytical solution gives a maximum tensile (compressive) stress which is constant in time. This behavior is due to the particular thermal boundary conditions adopted (which correspond to a similarity solution) in the mentioned semi-analytical study.
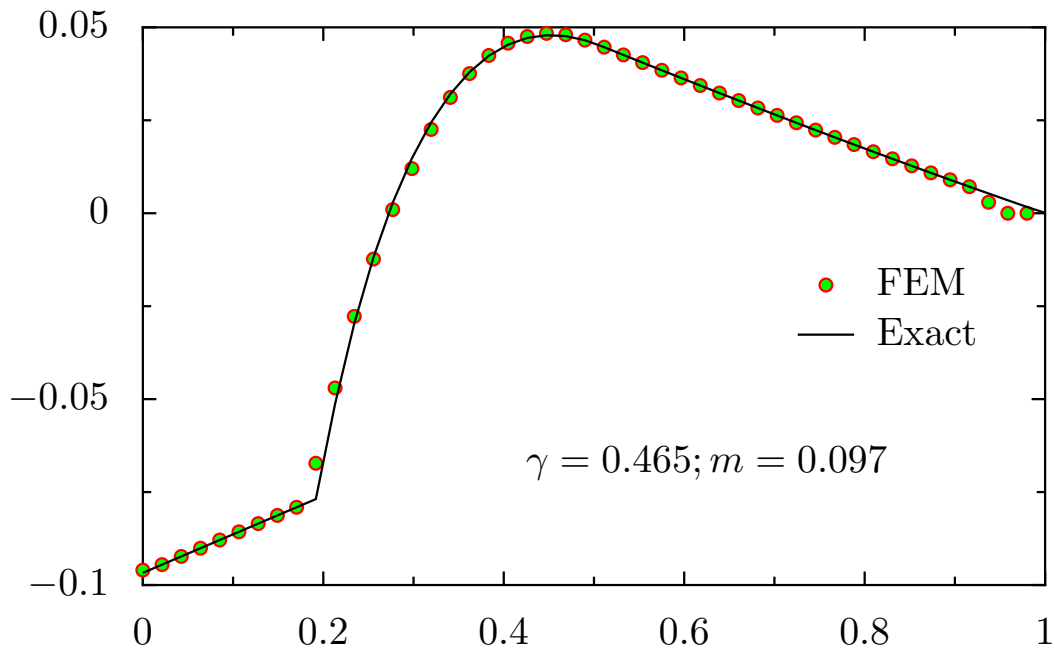
Figure 8: Stress distribution along the $\hat{y}$-coordinate. Comparison of semi-analytical[4] and numerical solutions.

5 THERMO-METALLURGICAL-MECHANICAL COUPLING SCHEME

The coupling is organized using a staggered scheme, where thermal, metallurgical and mechanical resolution follow on from each other at each time step, as shown in figure 9.

Any material property in the heat balance equation is temperature dependent and is assumed to be given by the mixture low described in §2.2 by equation (6) where $\hat{P} = \rho, C_p, \kappa$. Special treatment has been given to the latent heat associated to the austenite decomposition.

$$L = \sum_k L_k(T)\dot{y}_k(T, t) \tag{26}$$

where L_k is heat released during the transformation from austenite into the product k and $\dot{y}_k$ the volume fraction derivative with respect to time.

6 NUMERICAL EXAMPLE

In this section, we analyze the strain-stress field in a butt welded joint between strips of 0.3%C carbon steel.

Figure 10 gives a schematic diagram of the geometry and the finite element mesh. The x,y and z directions represent the length L, width W and thickness H of the strip.

In thermal and mechanical analysis the domain was discretized with linear tetrahedrons. The mesh was refined in the HAZ, and was coarsened gradually farther along the longitudinal direction.
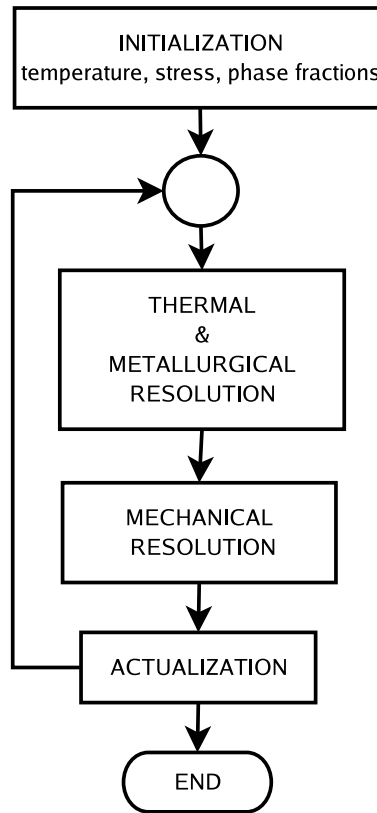
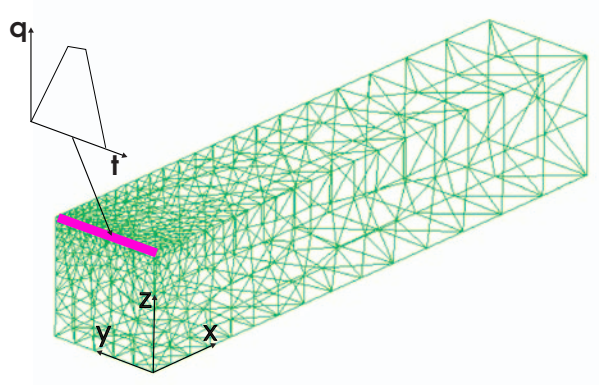Figure 9: Thermo-metallurgical-mechanical coupling scheme

Figure 10: Butt welded joint. Geometry and FEM mesh

The welding speed was assumed to be infinite. An external heat input is imposed in the edge marked in the figure 10. Initial temperature was defined at $To = 373\ K$, and all faces were defined as adiabatic boundaries, excepting that at $x = L$ where the temperature was fixed to $T_w = 373\ K$.

The mechanical boundary conditions were $u_z(0, y, 0) = 0, u_y(0, 0, 0) = 0, u_x(0, y, z) = 0,$
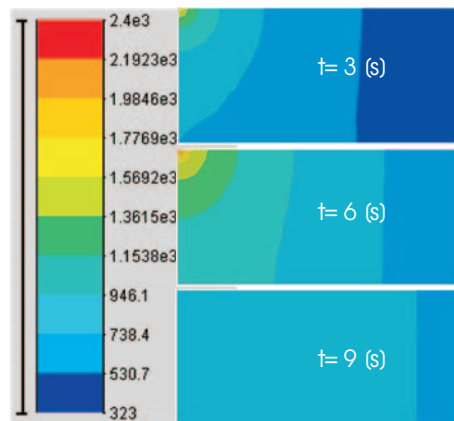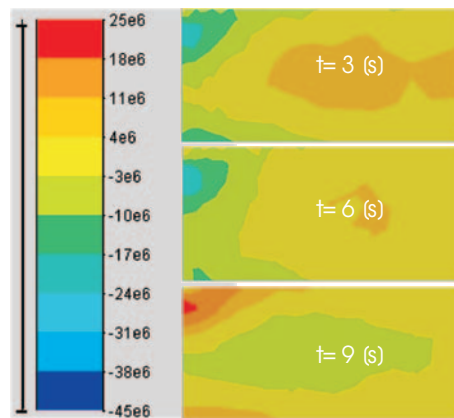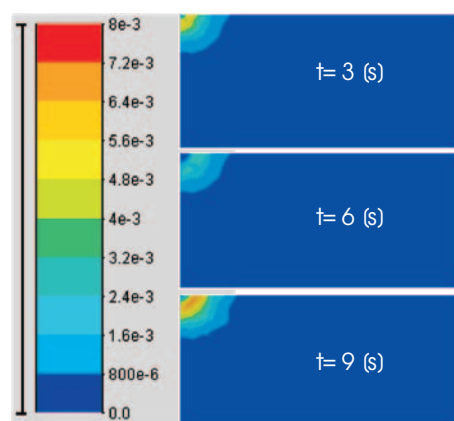
Figure 11: Butt welded joint. Temperature

Figure 12: Butt welded joint. σ_x stress

Figure 13: Butt welded joint. Equivalent plastic strain

assuming a symmetry condition in $x = 0$.

Figure 11 shows the temperature distribution, obtained with the thermal model previously developed and validated by the authors.[3]

The σ_x stress field is plotted in figure 12. Even when geometry and material properties were different, the distribution of tensile and compressive stresses compares well with several case studies published in the literature.[26]

The equivalent plastic strain is shown in figure 13.

7 CONCLUDING REMARKS

A model for thermomechanical analysis welding processes have been presented and discussed. The following conclusions are drawn from the study:

a) The model passed successfully the validations against the semi-analytical solutions of Osizik (thermal analysis of phase-change problems) and Weiner et al. (thermomechanical analysis of phase-change problems). This is a solid basement to continue the development of a software with ability to simulate accurately complex welding processes.

b) The metallurgical material model implemented in the program is able to model the evolution of thermal and mechanical properties associated with solid state phase transformations. This improves the accuracy of thermal and mechanical results, including the extent of the HAZ, the residual stress field and the cracking susceptibility.

Future work will include the development of computational tools for simulation of complex boundary conditions usually found in welding processes (like heat and mass transfer during the displacement of welding torches or electrodes), and also the implementation of more sophisticated non-linear mixture rules to determine material properties.

REFERENCES

[1] Mackerle J. Finite element analysis and simulation of welding-an addendum: a bibliography (1996-2001). *Modelling Simul. Mater. Sci. Eng.*, **10**, 295–318 (2004).

[2] Lindgren L. Finite element simulation of welding residual stresses and deformations. In Pollmann und Radaj, editor, *Simulation der Fugetechniken-Potentiale und Grenzen*. Daimler-Chrysler conference about welding simulations, Stuttgart, (2001).

[3] A. Anca, A. Cardona, and J.M. Risso. 3d-thermo-mechanical simulation of welding processes. *Mecánica Computacional*, **XXIII**, 2301–2318 (2004).

[4] J.H. Weiner and B.A. Boley. Elasto-plastic thermal stresses in a solidifying body. *J. Mech. Phys. Solids*, **11**, 145–154 (1963).

[5] Lindgren L. Finite element modelling and simulation of welding. part 2: Improved material modelling. *Journal of Thermal Stresses*, **24**(195-231) (2001).

[6] Özisik M. and Uzzell J. Exact solution for freezing in cylindrical symmetry with extended freezing temperature range. *Journal of Heat Transfer*, **101**, 331–334 (May 1979).

[7] J.O. Kristiansson. Thermal stresses in the early stage of solidification of steel. *J. of Thermal Stresses*, **5**, 315–330 (1982).

[8] J. M. Risso, A. E. Huespe, and A. Cardona. Thermal stress evaluation in the steel continuous casting process. *Int. J. Numer. Meth. Engng*, (2003).

[9] Melvin Avrami. Kinetics of phase change i. general theory. *J. Chem. Phys.*, **7**, 1103–1112 (1939).

[10] Melvin Avrami. Kinetics of phase change. ii transformation-time relations for random distribution of nuclei. *J. Chem. Phys*, **8**, 212 (1940).

[11] E. Scheil. Finite element modelling and simulation of welding. part 3: Efficiency and integration. *Archiv für Eisenhüttenwessen*, **8**, 565–567 (1935).

[12] S. J. Jones and H. K. D. H. Bhadeshia. Kinetics of the simultaneous decomposition of asutenite into several transfomation products. *Acta mater.*, **45**(7), 2911–2920 (1997).

[13] Tamas Reti, Zoltan Fried, and Imre Felde. Computer simulation of steel quenching process using a multi-phase transformation model. *Computational Materials Science*, **22**, 261–278 (2001).

[14] A. Cardona, I. Klapka, and M. Géradin. Design of a new finite element programming environment. *Engineering Computations*, **11**, 365–381 (1994).

[15] I. Klapka, A. Cardona, and M. Géradin. An object-oriented implementation of the finite element method for coupled problems. *Rev. Europ. Éléments Finis*, **7**(5), 469–504 (1998).

[16] J.C. Simo and T.J.R. Hughes. *Computational Inelasticity*. Springer, (1998).

[17] Hughes T. *The Finite Element Method. Linear Static and Dynamic Finite Element Analysis*. Prentice-Hall, (1987).

[18] Zienkiewicz O. and Taylor R. *The Finite Element Method*, volume 1: The Basis. Butterworth-Heinemann, 5th. edition, (2000).

[19] Cifuentes A. and Kalbag A. A performance study of tetrahedral and hexahedral elements in 3-d finite element structural analysis. *Fin. Elem. Anal*, **12**, 313–318 (1992).

[20] Benzley S., Perry E., Merkely K., Clark B., and Sjaardama G. A comparison of all hexagonal and all tetrahedral finite element meshes for elastic and elasto-plastic analysis. *Proc. 14th Ann. Int. Meshing Roundtable, Albuquerque, USA*, (1995).

[21] T. Nakagawa, T. Umeda, J. Murata, Y. Kamimura, and N. Niwa. Deformation behavior during solification os steels. *ISIJ Int.*, **35**(6), 723–729 (1995).

[22] A. Moitra, B. Thomas, and H. Zhu. Application of a thermo-mechanical finite element model of steel shell behavior in the continuous slab casting mold. *Proc.76th Steelmaking Conf. ISS*, **76**, 657–667 (1993).

[23] A. Yamanaka, K. Nakajima, and K. Okamura. Critical strain for internal crack formation in continuous casting. *Ironmaking and Steelmaking*, **22**(6), 508–512 (1995).

[24] Y.M Won, K.H. Kim, T. Yeo, and K.H. Oh. Effect of cooling rate on ZST, LIT and ZDT of carbon steels near melting point. *ISIJ Int.*, **38**(10), 1093–1099 (1998).

[25] C. Li and B. Thomas. Thermo-mechanical finite element model of shell behavior in the continuous casting of steel. *Proc.6th Asia-Pacific symp.on engineering plasticity and its applications*, **1**, 827–834 (2002).

[26] Li Yajiang, Wang Juan, Chen Maoai, and Shen Xiaoqin. Finite element analysis of residual stress in the welded zone of a high strength steel. *Bull. Mater. Sci.*, **27**(2), 127–132 (2004).